Journal of Cosmology and Astroparticle Physics

Detecting ALP wiggles at TeV energies

Journal of Cosmology and Astroparticle Physics
An IOP and SISSA journal

Received: *May 20, 2023*
Revised: *October 18, 2023*
Accepted: *December 7, 2023*
Published: *January 17, 2024*

Detecting ALP wiggles at TeV energies

M. Kachelrieß and J. Tjemsland

Institutt for fysikk, NTNU,
Trondheim, Norway

E-mail: michael.kachelriess@ntnu.no, physics@tjemsland.priv.no

Abstract: Axions and axion-like-particles (ALPs) are characterised by their two-photon coupling, which entails so-called photon-ALP oscillations as photons propagate through a magnetic field. These oscillations lead to distinctive signatures in the energy spectrum of high-energy photons from astrophysical sources, allowing one to probe the existence of ALPs. In particular, photon-ALP oscillations will induce energy dependent oscillatory features, or "ALP wiggles", in the photon spectra. We propose to use the discrete power spectrum to search for ALP wiggles and present a model-independent statistical test. By using PKS 2155-304 as an example, we show that the method has the potential to significantly improve the experimental sensitivities for ALP wiggles, and that the ALP wiggles may be detected using the Cherenkov Telescope Array (CTA) for optimistic values of the photon-ALP coupling constant and the magnetic field. Moreover, we discuss how these sensitivities depend on the modelling of the magnetic field. We find that the use of realistic magnetic field models, due to their larger cosmic variance, substantially enhances detection prospects compared to the use of simplified models.

Keywords: axions, gamma ray experiments, gamma ray theory

ArXiv ePrint: 2305.03604

https://doi.org/10.1088/1475-7516/2024/01/044

JCAP01(2024)044

Contents

1 Introduction

Axions are well motivated beyond the standard model particles that can explain a variety of unsolved problems in physics, such as the strong CP problem [1, 2] and the nature of dark matter [3–5]. These particles are mainly characterised by their two-photon coupling $g_{a\gamma}$ from the interaction term $\mathcal{L} = \frac{1}{4} g_{a\gamma} a F_{\mu\nu} \tilde{F}^{\mu\nu} = g_{a\gamma} a \boldsymbol{E} \cdot \boldsymbol{B}$, and by their small mass m_a obtained through pion mixing [6, 7]. The relationship between $g_{a\gamma}$ and m_a is thus fixed as $g_{a\gamma}\,\mathrm{GeV} \sim 10^{-16} m_a / \mu\mathrm{eV}$ up to a $\mathcal{O}(1)$ factor [8, 9]. A more general class of light pseudoscalar particles which share the same two-photon coupling as the axion but have an arbitrary mass m_a, is known as axion-like particles (ALPs). Although ALPs do not solve the strong CP problem, they are nevertheless interesting as they, e.g., arise naturally in string theories and other extensions of the standard model [10–12].

The majority of ALP searches are based on photon-ALP mixing in a magnetic field (see refs. [13, 14] for two recent reviews): Due to the characteristic two-photon-ALP vertex, a photon/ALP may interact with a virtual photon provided by the magnetic field and convert into an ALP/photon. Currently, the most solid and extensive exclusions at sub-eV masses, $g_{a\gamma} < 6.6 \times 10^{-11}\,\mathrm{GeV}^{-1}$, are set by the CAST helioscope ($m_a \lesssim$ eV) [15] by attempting to convert solar ALPs into photons on Earth. A comparable limit is found for $m_a \lesssim$ keV by studying the lifetime of horizontal branch stars [16, 17]. The planned "shining light through a wall" experiment ALPS-II [18] and the solar helioscope IAXO [19] are expected to improve upon these limits immensely. Significantly stronger limits around $m_{a\gamma} \sim 10^{-6}\,\mathrm{eV}$ are obtained for ALP dark matter in haloscope experiments, such as ADMX [20] and the upcoming ABRACADABRA experiment [21], or by conversion near neutron stars [22, 23].

JCAP01(2024)044

The strongest limits ($g_{a\gamma} \lesssim 10^{-11}$–$10^{-13}\,\mathrm{GeV}^{-1}$) at low masses ($m_a \lesssim 10^{-6}\,\mathrm{eV}$) are set by observations of astrophysical photon sources using the signatures that photon-ALP oscillations will imprint on photon spectra: First, photon-ALP oscillations will induce "irregularities". The non-detection of such spectral irregularities has been used to constrain the parameter space using, e.g., gamma-ray observations by HESS [24] and Fermi-LAT [25], observations of the Galactic diffuse gamma-rays by Tibet ASγ and HAWC [26], and using X-ray observations from Chandra [27–29]. The Cherenkov Telescope Array (CTA) is expected to improve the limits from HESS and Fermi-LAT [30]. Second, ALPs that are produced near or in the source can convert back into photons in, e.g., the Galactic magnetic field, thus inducing an additional gamma- or X-ray flux which has been searched for in SN1987A [31], Betelgeuse [32], and super star clusters [33]. Moreover, ALPs that are sourced near the polar caps in pulsars and resonantly converted to photons have recently been used to set leading limits [34]. Third, photon-ALP oscillations will increase the linear polarisation of photons, which can be used to set limits using e.g. optical photons or X-rays[1] from magnetic white dwarfs and neutron stars [36, 37]. In ref. [38], it was shown that the measurement of linear polarisation in white dwarf spectra excludes $g_{a\gamma} \gtrsim 5.4 \times 10^{-12}\,\mathrm{GeV}^{-1}$ for $m_a \lesssim 3 \times 10^{-7}\,\mathrm{eV}$, which is the strongest existing limit for ALP masses between $\sim 10^{-9}$ and $\sim 10^{-6}\,\mathrm{eV}$. At masses $m_a \lesssim 10^{-11}\,\mathrm{eV}$, the best limit is set by the non-detection of spectral irregularities in X-ray data from Chandra [27]. Finally, photon-ALP oscillations will effectively increase the mean-free path of photons at TeV energies since ALPs travel practically without any interactions with the extragalactic background light (EBL) [39]. This effect has been recently used to set strong limits with HAWC [40]. Moreover, this effect is important in combining fit analyses, such as in the recent limit set using FERMI flat radio quasars [41].

All the limits discussed in the previous paragraph are, however, strongly dependent on the treatment of the magnetic fields [42–45]. Therefore, one either needs a reliable description of the magnetic fields, or knowledge of how uncertainties in the magnetic fields affect the results (see e.g. the discussions in refs. [28, 46, 47]). This is particularly important for the turbulent component of the magnetic fields, since oversimplified models are often used to describe these fields.

In ref. [47] we introduced the idea of using the discrete power spectrum to probe photon-ALP oscillations in photon spectra. In this work, we further discuss and exemplify this concept. In particular, we introduce a statistical procedure that has the potential to significantly improve current detection prospects for irregularities induced by photon-ALP oscillations, which we name "ALP wiggles". The statistical method has two main applications: First, it can be used to search for ALP wiggles without specifying the EBL distribution and the magnetic field model. Second, the method is a convenient way to analyse the effect of various magnetic field models on the expected ALP wiggles. We find that this method is more robust than a standard χ^2 comparison with data.

In order to stay as concrete as possible, the examples focus on gamma-rays at TeV energies, of relevance for the upcoming CTA experiment. However, the same considerations and discussions also apply to other energy ranges, relevant for e.g. Fermi, HESS and Chandra.

[1] The same phenomenon occurs naturally also for gamma-rays, but the measurement of the polarisation is with current and planned detectors not possible [35].

JCAP01(2024)044

Furthermore, we only include the effect of the extragalactic magnetic field and fix $B_0 = 10^{-9}\,\mathrm{G}$ in section 3, while we use $B_0 = 5 \times 10^{-9}\,\mathrm{G}$ in section 4. Although these are (over-) optimistic choices for a space-filling, primordial magnetic field, the magnetic fields in filaments can easily reach higher values. For example, the turbulent and regular components of the magnetic fields in galaxies and clusters of galaxies are expected to be as large as $\mathcal{O}(10^{-6})\,\mathrm{G}$. In addition, we fix $g_{a\gamma} = 10^{-11}\,\mathrm{GeV}^{-1}$, which at $m_a \lesssim 10^{-6}\,\mathrm{eV}$ is excluded by a factor of ~ 2, and at $m_a \lesssim 10^{-11}\,\mathrm{eV}$ by more than an order of magnitude. Nevertheless, this choice is appropriate for our purposes: We advocate for a model independent approach to an ALP searches, since current limits based on astrophysical photon-ALP oscillations depend strongly on the modeling of the magnetic fields. Moreover, it suffice to show that the approach is more sensitive than the standard χ^2 search for residuals, which have already been used to set competitive and leading limits [24–29].

2 Photon-ALP oscillations in astrophysical magnetic fields

2.1 Equation of motion

Physically, one can interpret the photon-ALP oscillation as a mixing between two mass eigenstates, similar to neutrino oscillations. The mixing strength and oscillation length depend on the effective mass of the photon which in turn is determined by the propagation environment (i.e. the surrounding magnetic field, plasma, photon bath, etc.) and photon energy. A photon and an ALP with energy E propagating in z direction can be described by the linearised equation of motion [48],

$$(E + \mathcal{M} - \mathrm{i}\partial_z)\phi(z) = 0, \tag{2.1}$$

where $\phi = (A_\perp, A_\parallel, a)^\mathrm{T}$ is the wave function describing the two photon polarisation and ALP states. The mixing matrix can be written as

$$\mathcal{M} = \begin{pmatrix} \Delta_\perp & 0 & 0 \\ 0 & \Delta_\parallel & \Delta_{a\parallel} \\ 0 & \Delta_{a\parallel} & \Delta_a \end{pmatrix}, \tag{2.2}$$

where $\Delta_{\perp/\parallel} = (n_{\perp/\parallel} - 1)E$ (n being the refractive index of the photon), $\Delta_a = -m_a^2/(2E)$ and $\Delta_{a\gamma} = g_{a\gamma} B_\mathrm{T}/2$. The transverse magnetic field $\boldsymbol{B}_\mathrm{T}$ is the component of the magnetic field perpendicular to the propagation direction, and the index $\perp$ ($\parallel$) refers to the direction perpendicular (parallel) to $\boldsymbol{B}_\mathrm{T}$.

In this work, we consider only photons in the sensitivity range of CTA ($\sim 10^{11}$–$10^{14}\,\mathrm{eV}$) and low ALP mass ($m_a \lesssim 10^{-10}\,\mathrm{eV}$). Then the dominant contribution to the photon refractive index is the one from the EBL [47], given by [49]

$$\Delta_\mathrm{EBL} \simeq \Delta_\mathrm{CMB} \simeq 0.5 \times 10^{-42} E. \tag{2.3}$$

All turbulent magnetic fields lead to similar dependencies on the oscillation parameters [47], and the discussions in this paper can therefore be applied to other energy ranges and magnetic field.[2]

[2]For example, at X-ray energies and small axion masses, the astrophysical photon-ALP oscillations are determined mainly by the plasma density, for which $\Delta_\mathrm{pl} \propto E^{-1}$.

JCAP01(2024)044

2.2 ELMAG

We simulate the propagation of photons using ELMAG [50, 51] which is a Monte Carlo program that simulates electromagnetic cascades of high-energy photons, electrons and positrons created by their interactions with the EBL. We have implemented ALPs into ELMAG [47], thereby allowing for a consistent treatment of cascading and oscillations. This advantage is however at the cost of being significantly more computationally demanding than the alternative Python packages GammaALP [52] and ALPro [28], which are based on transfer matrices.

Compared to ref. [47] we have added the following features ELMAG:[3] Gaussian turbulent fields with a broken power-law as power spectrum [see eq. (2.4)] can be modelled, the magnetic field strength can be distributed as a top-hat function with a given filling factor, and the computation time is significantly reduced.

2.3 Magnetic field models

High-energy photons will encounter a variety of turbulent magnetic fields on their path towards Earth, with strengths varying from $B \sim 1\,\mathrm{G}$ near jets of AGNe, fields on galactic scales with $\sim \mu$G, within galaxy clusters (~ 0.1–$10\,\mathrm{nG}$) and finally the intergalactic magnetic field, see e.g. refs. [53, 54] for recent reviews. The energy in the turbulent magnetic fields in galaxies and galaxy clusters are believed to be generated at large scales 0.1–10 kpc through, e.g., "mechanical stirring", large- and small-scale dynamos, and compression. The energy is in turn transported to smaller length scales through an energy cascade, leading to a power-law spectrum of the turbulent magnetic field. It is common to assume that the magnetic field either has a Kolmogorov ($\gamma = -5/3$) or Kraichnan ($\gamma = -2/3$) spectrum. At small k, a Batchelor spectrum ($\beta = 5$) is expected, but other spectral indices have been suggested too.

In order to take into account the stochastic nature of the turbulence, we will describe it as a divergence-free Gaussian turbulent field with zero mean and RMS-value $B_{\mathrm{rms}}^2 = \langle B^2 \rangle$. Following the approach of refs. [55, 56], we describe the magnetic field as a superposition of n left- and right-circular polarised Fourier modes. The modes will be distributed according to the power-law spectrum

$$B_j = B_{\mathrm{min}} \left(\frac{k_j}{k_0}\right)^{\beta/2} \left[1 + \left(\frac{k_j}{k_0}\right)^{\gamma+\beta}\right]^{-1/2} \tag{2.4}$$

between k_{min} and k_{max}. The parameter k_0 determines the break in the power law which is visible in the magnetic field spectra shown in figure 1. In the case of astrophysical magnetic fields, $L_0 = 2\pi/k_0$ corresponds to the injection scale. The field modes extend down to the dissipation scale $L_{\mathrm{min}} = 2\pi/k_{\mathrm{max}}$ which is below any astrophysical scale of interest. In practise, one cuts off therefore the spectrum at a value of L_{min} which is much smaller than the smallest relevant scale of the problem in question.[4] We use $k_{\mathrm{max}} = 100 k_0$, fix k_{min} by the condition $B(k_{\mathrm{min}}) = B(k_{\mathrm{max}})$ and use 33 modes per decade. The field is normalised such that $B_{\mathrm{rms}}^2/2$ coincides with the energy density stored in the field. We define the coherence

[3] The code will be made publicly available in a future release of ELMAG.

[4] Here, the largest relevant wave number is $k_{\mathrm{osc}} = \Delta_{\mathrm{CMB}}(10^{14}\,\mathrm{eV}) \sim 8\,\mathrm{Mpc}^{-1}$.

JCAP01(2024)044

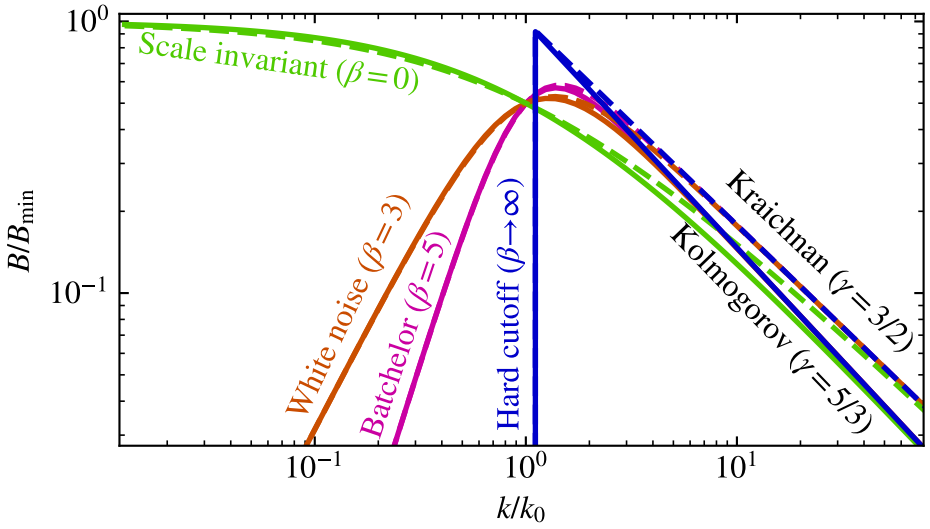

Figure 1. Visualisation of different magnetic field spectra that can be modelled in `ELMAG`.

length $L_{\rm c}$ of the turbulent fields as

$$L_{\rm c} = \frac{\pi}{B_{\rm rms}^2} \int \frac{{\rm d}k}{k} \boldsymbol{B}^2(k). \tag{2.5}$$

For comparison, we will also consider a simple domain-like field which is often used in the literature due to its simplicity [27, 29, 57–61]. In this approach, the magnetic field is split into patches with a size equal to the coherence length $L_{\rm c}$. Within each patch, the magnetic field is homogeneous with a randomly chosen direction. This model is unphysical and may lead to a bias in the strength of the ALP signatures deduced [46, 47].

As already mentioned, we will focus on the effect of the intergalactic magnetic field. From the non-detection of electromagnetic cascades from blazars, it was concluded that the extragalactic space must be filled with an turbulent magnetic field with a strength of $B \gtrsim 10^{-14}\,{\rm G}$ with a large filling factor [62–64], while an upper limit of $B \lesssim 10^{-9}\,{\rm G}$ is derived from Faraday rotation measurements [65]. The nature and the production of the extragalactic magnetic field remain however unknown: A large range of magnetic field strengths, spectral index at small k (i.e. β) and coherence lengths are made possible by the many conceivable production mechanisms. For example, if produced during inflation, the initial magnetic spectrum will be scale invariant ($\beta = 0$). Its coherence length is currently limited by hydrodynamical turbulence decay from below ($\sim$ kpc) and the Hubble radius from above. Meanwhile, the range of allowed magnetic field strengths is slowly closing, and it has been argued that the remaining parameter space can be completely eliminated by the non-detection of magnetic halos from misaligned blazars [66]. As a solution, ref. [66] proposed that the electromagnetic cascades are quenched by plasma instabilities, what, if confirmed, would re-open large parts of the parameter space for intergalactic magnetic fields.

In the remaining of this work, we will focus on the effect of a primordial intergalactic magnetic field with a field strength $B \sim 10^{-9}\,{\rm G}$. This value is chosen to highlight the signatures and the effect of the statistical method introduced in section 3.3. Although this

JCAP01(2024)044

value is arguably over-optimistic for primordial fields, similar field strengths can easily be obtained in filaments between clusters of galaxies, or in Galactic magnetic fields which we for concreteness do not include. Although we consider only TeV photons, all of the discussions and considerations made in this paper can be applied to other energies and astrophysical environments [47], taking into account that the energy dependence of the refractive index scales as E^{-1} at low energies and as E^{1} at high energies. Due to the many uncertainties, and since the expected signal depends strongly on the treatment of the magnetic fields, we will in this work advocate for an experimental approach independent of the modelling of the magnetic fields and the source spectrum.

2.4 Parameter space

Photon-ALP oscillations will lead to two important signatures on high-energy photon spectra at $E \sim$ TeV. First, they will perturb the photon spectrum by energy dependent oscillations with $k \sim \Delta_{\rm osc}$ [see eq. (2.6)], even for a turbulent magnetic field [47]. Second, the mean free path length of photon will increase since ALPs will propagate without interacting with the EBL. In this work, we focus on the former effect. In this subsection, we will estimate the ALP and magnetic field properties needed to observe ALP wiggles with CTA, and motivate our focus on intergalactic magnetic fields. The conditions discussed here can be deduced graphically from figure 3 in ref. [47].

For a homogeneous magnetic field, the oscillation probability is given by

$$P_s(\gamma \to a) = \left(\frac{2\Delta_{a\gamma}}{\Delta_{\rm osc}}\right)^2 \sin^2\left(\Delta_{\rm osc} s/2\right) \tag{2.6}$$

with $\Delta_{\rm osc}^2 = (\Delta_{\parallel} - \Delta_a)^2 + 4\Delta_{a\parallel}^2$. The oscillation length is then defined as $L_{\rm osc} = 2\pi/\Delta_{\rm osc}$. The oscillatory features — which we name "ALP wiggles" — described by the solution in eq. (2.6) are present also in turbulent magnetic fields provided that the coherence length is on the same order of magnitude or larger than the oscillation length. At TeV energies, this happens when $2\pi/\Delta_{\rm CMB} \lesssim L_{\rm c}$, or

$$E \gtrsim 8 \times 10^{12}\,{\rm eV} \left(\frac{L_{\rm c}}{10\,{\rm Mpc}}\right)^{-1}. \tag{2.7}$$

The coherence length of the intergalactic magnetic field is practically unconstrained from above, for concreteness we will use $L_{\rm c} \sim 5\,{\rm Mpc}$ as default value. Meanwhile, the Galactic magnetic field has a turbulent component which coherence length is usually assumed to be around 20 pc, and the regular component should be comparable to the size of the Galaxy, $\sim 10\,{\rm kpc}$. Thus, the turbulent component of the Galactic magnetic field is expected to contribute little to the ALP wiggles at CTA energies.

The ALP wiggles are most prominent around the transition from the strong mixing regime, occurring when $\Delta_{\rm CMB} \sim \Delta_{a\gamma}$ or

$$E^{\rm crit} \simeq 2 \times 10^{11}\,{\rm eV} \times \frac{g_{a\gamma} B}{10^{-11}\,{\rm GeV}^{-1}\,{\rm nG}}. \tag{2.8}$$

Since CTA is most sensitive in the range between 10^{11} and $10^{14}\,{\rm eV}$, one should ideally have $10^{11}\,{\rm eV} \lesssim E^{\rm crit}$. This yields

$$\frac{g_{a\gamma} B_{\rm T}}{10^{-11}\,{\rm GeV\,nG}} \lesssim 1/2. \tag{2.9}$$

JCAP01(2024)044

Furthermore, the ALP mass should be small enough that there exists a strong mixing regime for the given magnetic field strength. This leads to the condition $m_a \lesssim 10^{-10} B_{\rm T}/{\rm nG}$. Since the onset of the wiggles is determined by the weakest magnetic field and photon spectra are usually steeply falling, the intergalactic magnetic field may prove to lead to the strongest wiggles.

In eqs. (2.8) and (2.9), only the combination $g_{a\gamma} B_{\rm T}$ is of importance. This implies that if we change $g_{a\gamma}$ or $B_{\rm rms}$, we will change the energy at which the wiggles are most prominent — weaker magnetic fields or lower $g_{a\gamma}$ implies that we should look at lower energies with a different detector. However, the exact morphology and distribution of magnetic field strengths is unknown. In general, a combination of the Galactic magnetic field ($B = \mathcal{O}(\mu{\rm G})$), magnetic fields around galaxy clusters ($B = \mathcal{O}(\mu{\rm G})$), and the extragalactic magnetic field ($B = 10^{-9}$–$10^{-14}\,{\rm G}$) will influence ALP oscillations. Therefore, in the next two sections, we introduce and advocate for a search for ALP wiggles in which the magnetic field does not need to be specified. The example parameters that will be used are chosen such that the wiggles will be prominent in the CTA energy range ($g_{a\gamma} = 10^{-11}\,{\rm GeV}$, $B_{\rm rms} = 10^{-9}$ [section 3], $B_{\rm rms} = 5 \times 10^{-9}$ [section 4]), and the results should therefore only be considered as a proof of principle.

3 Statistical tests for ALP wiggles

3.1 The χ^2 test for irregularities

The ALP wiggles induced by photon-ALP oscillations will be perceived as "irregularities" in the photon spectrum. Thus, one can use as a probe the χ^2 test,

$$\chi^2 = \frac{1}{N_{\rm bins} - 1} \frac{[f_{\rm data}(E) - f(E)]^2}{\sigma^2_{\rm data}}, \tag{3.1}$$

where $f_{\rm data}(E)$ is the measured binned energy spectrum (with photon-ALP oscillations if they exist), $\sigma_{\rm data}$ is the experimental uncertainty, $N_{\rm bins}$ is the number of data points, and $f(E)$ is the modelled spectrum (without ALP oscillations) [59]. However, even though this method is statistically sound, it can only measure whether the photon spectrum is more irregular than statistically expected. In the simulated examples in this work we 'model' instead the spectrum by fitting the function

$$f(E) \propto E^{-b} \exp\{-\tau(E)\}\,, \qquad \text{with} \qquad \tau = \exp\{\beta(\log(E))\} \tag{3.2}$$

where $\beta(x)$ is a fifth order polynomial and b is the spectral index[5] to the un-binned spectra by minimising the maximum likelihood estimate (MLE) in order to isolate the effect of the wiggles in a model independent way.

3.2 The discrete power spectrum

The photon-ALP oscillations will perturb the photon spectrum by energy dependent oscillations, $k \sim \Delta_{\rm osc}$, even for a turbulent magnetic field. At energies above the strong mixing regime, the ALPs with thus lead to wiggles with $k \sim E$ in the observed photon spectra.

[5] Due to the high degeneracy of the fit, we fix for simplicity b to the simulated value.

JCAP01(2024)044

Likewise, below the strong mixing regime, the wiggles have the wavenumber $k \sim E^{-1}$. In ref. [47], we suggested therefore to use the windowed discrete power spectrum,

$$G_N(k) = \left| \frac{1}{N} \sum_{\text{events}} \mathrm{e}^{\mathrm{i}\eta k} \right| , \tag{3.3}$$

to extract information on the wiggles. The sum in eq. (3.3) goes over the N detected photon events. Only photons with energies between $E_{\min}$ and $E_{\max}$ are included, and we use $\eta = E/E_{\min}$ to resemble the expected energy dependence of the wiggles above the strong mixing regime. A similar concept was introduced in ref. [67]. Importantly, one can use the discrete power spectrum to search for ALPs without specifying the magnetic field. However, for a turbulent magnetic field, the ALP signal is a broadened peak whose location and width is a priori unknown. While this makes a detection more challenging, it enables the extraction of information on the magnetic field.

Note that the signal strength depend on the choice of $E_{\min}$: It should be chosen close to the transition from the strong mixing regime, which a priori is unknown. This means, on the other hand, that the conditions (2.7) and (2.9) can in principle be used to deduce the ALP parameters from a detected photon-ALP oscillation signal: The combination $g_{a\gamma}B_{\perp}$ will for most astrophysical environments determine the onset of the oscillations $\Delta_{\text{CMB}} = 2\Delta_{a\parallel}$ (see figure 3 in ref. [47]). This means that $g_{a\gamma}B_{\perp}$ can be fixed by finding the value of $E_{\min}$ that optimises the observed oscillations. The mass m_a can likewise be determined by X-ray measurements.

We consider the test statistic (TS) given by the goodness-of-fit measure compared to an estimated background,

$$\text{TS} = \frac{1}{\Delta k} \int_0^{\Delta k} \frac{[G_N(k) - G_N^B(k)]^2}{\sigma_N^B(k)^2} \, \mathrm{d}k \, . \tag{3.4}$$

Here, $G_N^B(k)$ and $\sigma_N^B(k)$ are the estimated background power spectrum and its 1σ variation (see section 3.3). We choose $\Delta k = 6$ to reduce the contributions from random fluctuations at large k. While eq. (3.4) shares similarities with the χ^2 statistics, one should emphasise that one expects a longer tail in this test statistics since we are integrating over a range in which there statistically is expected to be random peaks, i.e. the probability that there is a random peak at any k is larger than the probability that there is a peak at a fixed k. The TS can in principle be improved if the shape, position and width is taken into account, using for example machine learning.

3.3 Statistical procedure and examples

In this section, the use of the discrete power spectrum to detect ALP wiggles will be exemplified. We will focus on the effect of the magnetic field modelling on the ALP wiggles, thereby illustrating the importance of a proper treatment of the magnetic fields in modelling photon-ALP oscillations. Based on the discussions above, we define the following statistical procedure:

1. Photons are sampled according to the chosen source spectrum using `ELMAG`. The simulations are stopped when a given number N of photons has reached the detector within the considered energy range. The energy of the simulated photons that reached the detector is used to compute the discrete power spectrum G.

JCAP01(2024)044

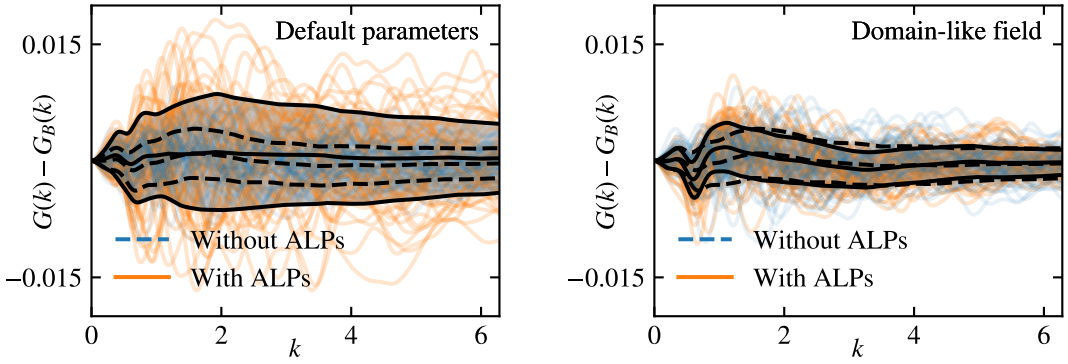

Figure 2. The power spectrum with the estimated background subtracted is plotted using a Gaussian turbulent field (left) and a domain-like field (right). The results for 50 realisation of the magnetic field with (orange) and without (blue) photon-ALP oscillations is shown, and the averages and the statistical standard deviations from a sample of 10^3 realisations are shown in black lines. The parameters used in the simulations are discussed in the main text.

2. The "measured spectrum" is modelled by minimising the maximum-likelihood-estimate (MLE) of the fit function (3.2) to the simulated data.

3. The background power spectrum and its statistical variation is in turn found by drawing $N \times 10^3$ energies using the fitted spectrum as a probability distribution.

4. The TS is computed using (3.4).

In all the scenarios considered in this section, we repeat this procedure for 10^3 realisations of the magnetic field in order to obtain the distribution of TS values.

For concreteness, we will consider $N = 10^4$ detected photons and in the energy range $E \in (10^{12}, 10^{14})\,\mathrm{eV}$ with the injection spectrum $\mathrm{d}N/\mathrm{d}E \propto E^{-1.2}$. Moreover, we fix $g_{a\gamma} = 10^{-11}\,\mathrm{GeV}^{-1}$ and use a turbulent magnetic field with $B_{\mathrm{rms}} = 5\,\mathrm{nG}$. The power spectrum using a Gaussian turbulent field with $\gamma = 5/3$, $\beta \to \infty$ and $L_{\mathrm{c}} = 5\,\mathrm{Mpc}$ (default parameters) is shown in the left pane of figure 2. In all plots in this section, the various scenarios will be labelled using the parameters that differs from the default parameters. The results for 50 realisations with photon-ALP oscillations are shown in orange lines, those without photon-ALP oscillations in blue. The averages and the 1σ statistical variance (black lines) were computed using the full set of 10^3 realisations. For comparison, the results using a domain-like field are shown in the right pane of figure 2.

The results in figure 2 show the power of the statistical procedure: There are clear peaks in the power spectrum including photon-ALP oscillations compared to the case without photon-ALP oscillations.[6] Interestingly, due to the lack of cosmic variance in the simple domain-like field, there is a lack of variance in the photon spectra which represents itself as a clear signal in the discrete power spectrum, even after averaging over many realisations of the

[6]Note that there is a minor bump, still comparable with flat, in the power spectrum without any photon-ALP oscillations. This indicates that our fit function does not perfectly describe the optical depth of the used EBL model. For the purposes of this paper, where the fitting procedure is made automatic using $\mathcal{O}(10^4)$ spectra, the quality of the fit is sufficient.

JCAP01(2024)044

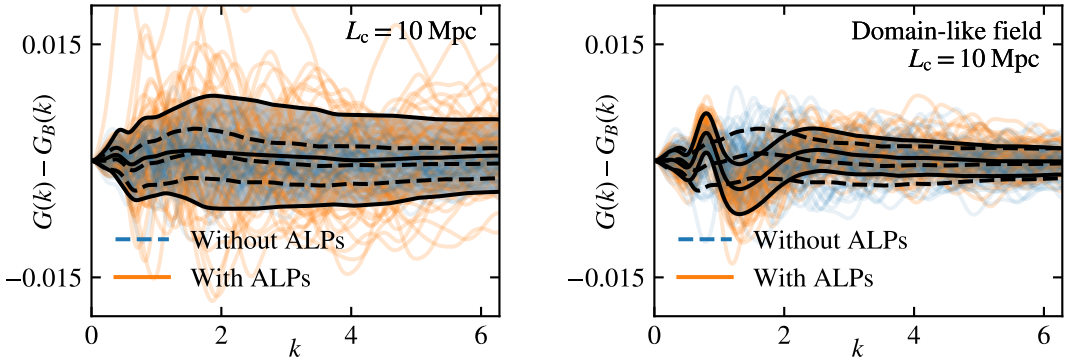

Figure 3. Same as figure 2, but with $L_c = 10\,\mathrm{Mpc}$.

magnetic field. This becomes even clearer for larger coherence lengths, as shown in figure 3 for $L_c = 10\,\mathrm{Mpc}$. As such, the use of simplified magnetic field models, such as the domain-like field, may lead to a bias in searches for ALP wiggles and impact the estimated limits on $g_{a\gamma}$. However, the larger variance in more realistic magnetic field models — in these examples represented by Gaussian turbulent fields — increases the rate of random encounters of regions of magnetic fields that may enhance the wiggles (see also the discussion in, e.g., ref. [68]). Thus, a more realistic modelling of the magnetic fields may, in fact, improve the detection prospects by such random encounters. The detection prospects could be further improved choosing more suitable fitting functions. Moreover, a constant windowing function was used. By varying the minimal energy, E_{min}, one may hope to further increase the detection sensitivity

For visualisation and to better understand the essence of the method, we plot in figure 4 the binned energy spectrum (green errorbars) and the fitted[7] spectrum (blue dashed line) for one random realisation of the magnetic field, both with and without photon-ALP oscillations. In addition, the spectrum averaged over all simulations and its standard deviation is shown (orange region). It is clear that photon-ALP oscillations increase the variation in the energy spectrum. The task of the generic fitting function (3.2) is to reduce the effect of unknown features in the source spectrum, such as uncertainties in the modelling of the EBL or unresolved features in the source spectrum. This leads to a caveat of this approach, well visualised in figure 4 with the spectrum that yielded the highest TS value in this analysis: The spectrum may be "over-fitted", i.e. part of the signal will be incorporated into the fit function, weakening thereby the signal. This applies especially for the wiggles extending over a larger energy range. Since the true injection spectrum of the source is not known, a detailed modelling of the source would be required in such cases to distinguish between intrinsic and ALP induced features in the energy spectrum.

In figure 5, we plot the distribution of the TS (3.4), for the default parameters, $L_c = 1\,\mathrm{Mpc}$, $L_c = 10\,\mathrm{Mpc}$, and a domain-like field. With the chosen TS, the domain-like field is difficult to distinguish from the non-ALP scenario. The Gaussian turbulent field, however, has a clear tail in the TS distribution, which distinguishes the ALP from the non-ALP scenario. While increasing the coherence length improves the detection prospects, details of the magnetic field like the values of γ and β have only a minor influence on the TS distribution and we therefore

[7] We emphasise that un-binned data are used in the fit.

JCAP01(2024)044

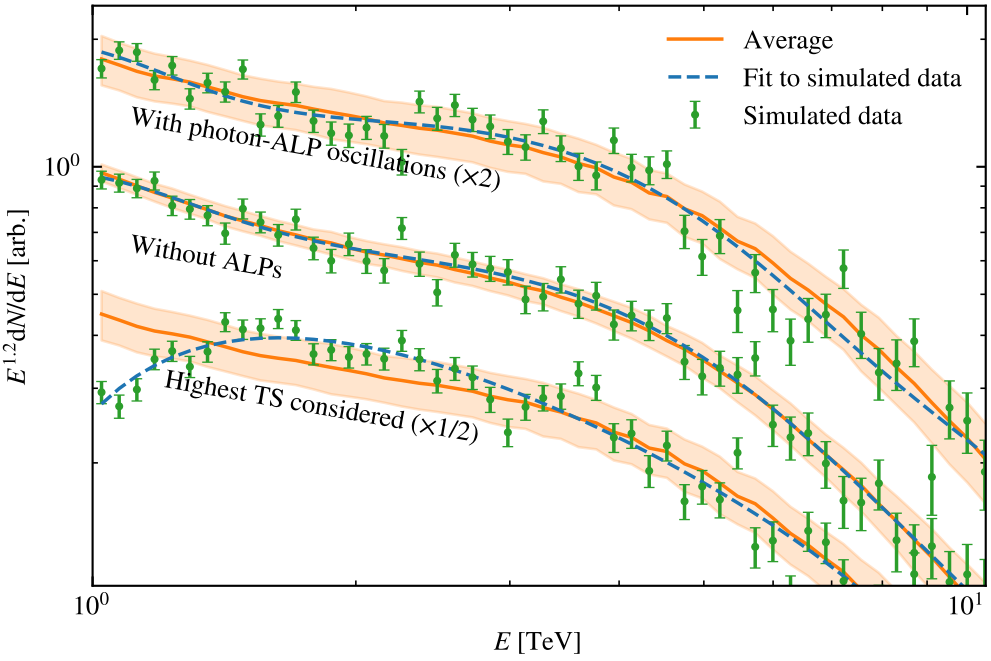

Figure 4. The simulated data (green errorbars) for one random realisation of the magnetic field are plotted with and without photon-ALP oscillations. The spectra are multiplied by a constant to improve visibility. Furthermore, the function (3.2) fitted to the (un-binned) data is shown as a blue dashed line together with the average obtained from the complete sample of 1000 realisations is shown. In addition, the spectrum from the simulation that yielded the highest TS is shown.

do not vary them in the figure. The reason for the weak dependence on these parameters is that the integrated magnetic field distributions, or the filling factor, is independent of the magnetic field spectrum for a Gaussian turbulent field with the same B_{rms} and L_{c}. In order to more clearly quantify the differences, we list in table 1 the probability that a signal is detected with a confidence level of 2σ, denoted as C_{95}, and the 99 % quantile for the various magnetic field scenarios considered. Although there are only minor differences in the C_{95} value, there are noticeable differences in the tails of the distributions, registered in the 99 % quantiles.

Note that the results of our examples clearly show that the sensitivities depend strongly on whether a Gaussian turbulent or a domain-like field is used: Due to the cosmic variance in more realistic magnetic field models, there is a chance that photons and ALPs propagate through a region of magnetic fields favourable for photon-ALP oscillations, thus enhancing the probability for detection. The same conclusion can be drawn by, e.g., the results in ref. [43] wherein limits where set using a domain-like magnetic field and using cosmic MHD simulations. Likewise, in ref. [68], it was found that cosmic MHD simulations have a larger change of such "rare encounters" than a Gaussian turbulent field. Thus, using a more realistic field than the Gaussian magnetic field considered here may improve the sensitivities even further.

JCAP01(2024)044

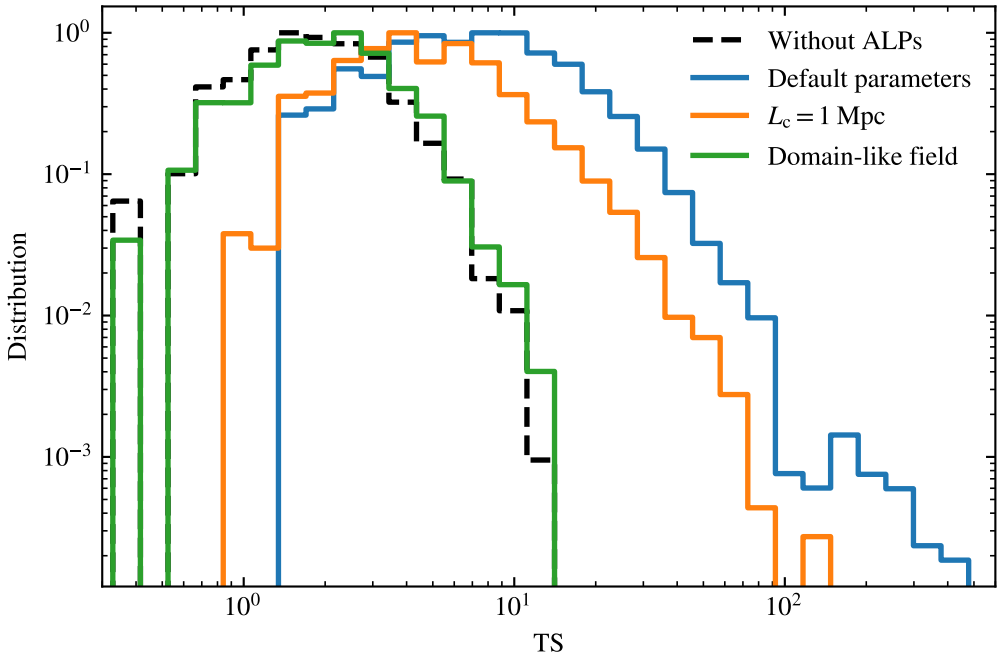

Figure 5. Histograms of the TS (3.4) obtained using the statistical method described in subsection 3.3. The various colored lines are obtained using different parameters for the magnetic field; the labels indicate the parameter changed compared to the default parameters (see the main text for a description). The results in the no-ALP scenario is plotted as a dashed black line.

Parameter	C_{95}	99 % quantile
Default	0.984	98.3
$\gamma = 4/3$	0.989	135
$\gamma = 2$	0.989	101
$\beta = 2$	0.988	183
$\beta = 4$	0.991	183
$f = 0.1$	0.988	69.9
$L_c = 1\,\mathrm{Mpc}$	0.955	50.2
$L_c = 10\,\mathrm{Mpc}$	0.972	140
Domain-like field	0.628	9
Domain-like $L_c = 10\,\mathrm{Mpc}$	0.660	10

Table 1. The probability that a signal is detected with a confidence level of 2σ, denoted as C_{95}, for the various magnetic field scenarios considered with eq. (3.4) as TS.

JCAP01(2024)044

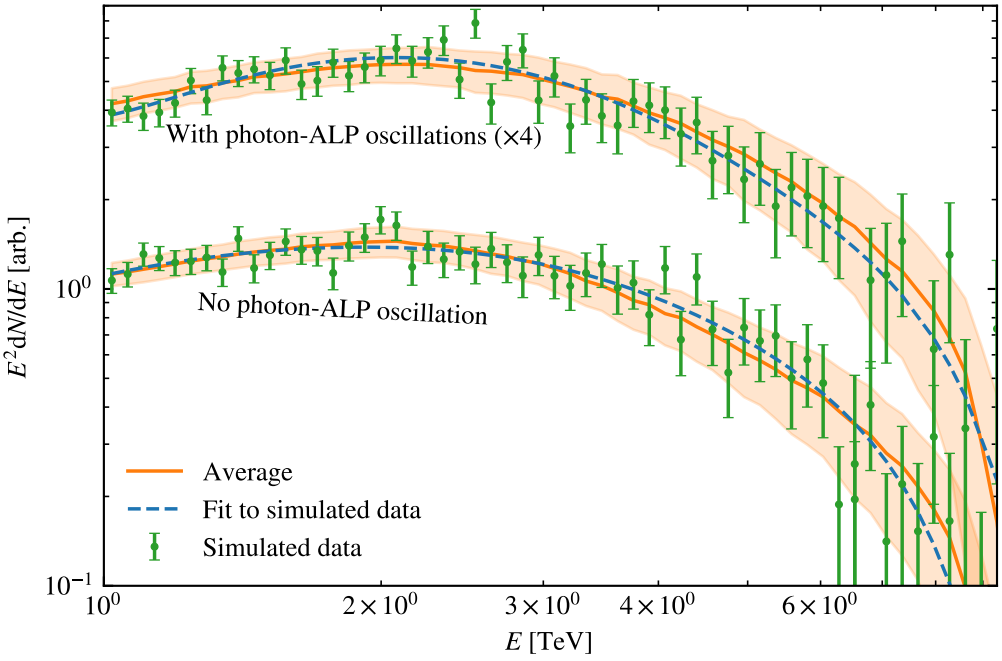

Figure 6. Same as figure 4, but with $N = 2.6\times10^3$ photons and the parameters used for PKS 2155-304.

4 Detecting ALP wiggles from PKS 2155-304 with CTA

In this section, we will consider PKS 2155-304 [69] at redshift $z = 0.116$ as a concrete example. Its photon spectrum can be approximated by [70]

$$\frac{\mathrm{d}N}{\mathrm{d}E} = N_0 \left(\frac{E}{E_b}\right)^{-\alpha-\beta\log(E/E_b)}, \tag{4.1}$$

with $N_0 = 15.4\times10^{-12}\,\mathrm{cm^{-2}s^{-1}MeV^{-1}}$, $E_b = 1136\,\mathrm{MeV}$, $\alpha = 1.77$ and $\beta = 0.035$. Since CTA [71] is not yet operational and its sensitivities are preliminary, we assume conservatively an energy-independent effective collection area $A = 10^5\,\mathrm{m}^2$. We take, however, into account the energy resolution of the detector by scrambling the detected energies using a normal deviate with an energy dependent half-width given by the preliminary energy resolution of CTA. Furthermore, we consider an energy range $E \in [10^{12}, 10^{14}]\,\mathrm{eV}$, for which the energy resolution $\Delta E/E$ is approximately energy independent.[8] The expected number of photons detected by CTA in this energy range from PKS 2155-304 can then be approximated as

$$N = A\Delta t \int \mathrm{d}E\ \frac{\mathrm{d}N}{\mathrm{d}E} \approx 2.6\times10^3 \left(\frac{\Delta t}{50\,\mathrm{h}}\right)\left(\frac{A}{10^5\,\mathrm{m}^2}\right), \tag{4.2}$$

A being the effective detector area and Δt the detection time. In figure 6, we plot the spectrum obtained from one simulation of PKS 2155-304 for an observation time $\Delta t = 50\,\mathrm{h}$ and a Gaussian turbulent field with $L_\mathrm{c} = 5\,\mathrm{Mpc}$.

To get an idea of the detectability of ALP wiggles from PKS 2155-304, we follow the statistical procedure from section 3.3. The result is shown in figure 7 for observation times

[8] If the larger energy range $E \in [10^{11}, 10^{14}]\,\mathrm{eV}$ is used, one should convolve a parametrisation of the energy resolution with the fit function.

JCAP01(2024)044

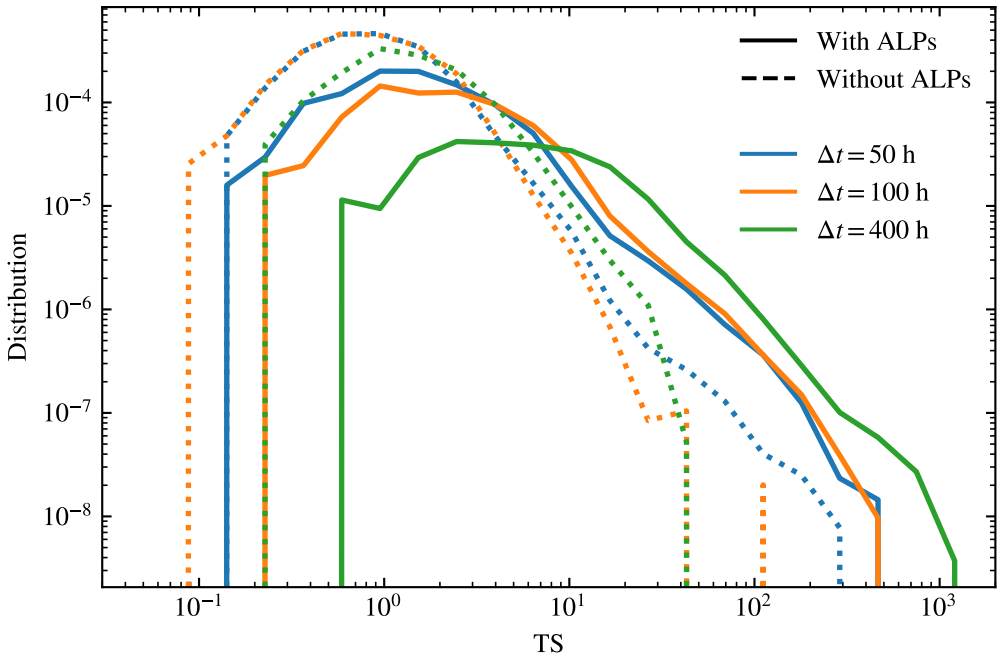

Figure 7. Histograms of the TS (3.4) obtained using the statistical method described in subsection 3.3 on the simulated data from PKS 2155-304 for the observation times $\Delta t = 50$ h (blue), 100 h (orange), 200 h (green) and 400 h (red). The corresponding no-ALP cases are shown with dashed lines.

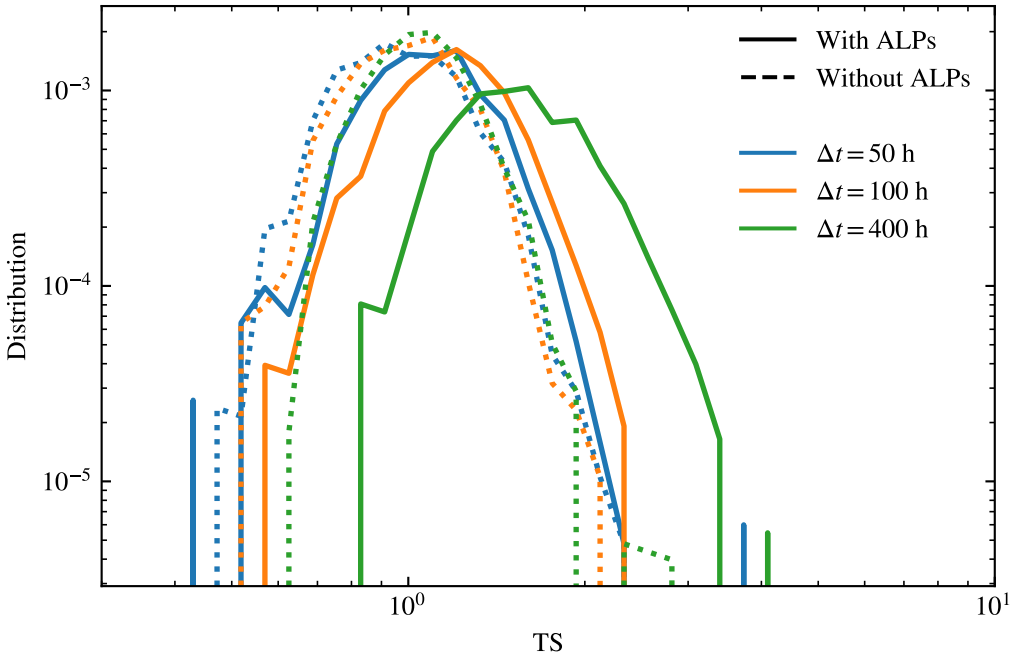

Figure 8. Same as figure 7, but with the χ^2 value [eq. (3.1)] as TS.

$\Delta t = \{50, 100, 400\}$ h. As expected, increasing the observation time increases the detection prospects. As a basis for comparison, we consider in figure 8 the TS distribution using eq. (3.1) with the same binning as in figure 6.

JCAP01(2024)044

	$\Delta t = 50\,\mathrm{h}$	$\Delta t = 100\,\mathrm{h}$	$\Delta t = 200\,\mathrm{h}$	$\Delta t = 400\,\mathrm{h}$
Power spec.	0.218	0.469	0.591	0.644
Spec.	0.094	0.228	0.478	0.597

Table 2. The table indicates the probability that ALPs are detected in an observation of PKS 2155-304 using CTA with a confidence level larger than 2σ, denoted as C_{95}, using the power spectrum [eq. (3.4)] and a standard χ^2 search [eq. (3.1)]. The columns corresponds to the detection times used in figure 7.

In order to more clearly quantify the differences between the statistical methods used in figures 7 and 8, we list in table 2 the probability that a signal is detected with a confidence level of 2σ, denoted as C_{95}, for the various magnetic field scenarios considered. From these values, we conclude that the use of the discrete power spectrum leads to better detection prospects compared to a standard irregularity search in the energy spectrum, especially for low observation times. Note, however, that the search for irregularities will depend on the binning, and can thus be improved. On the flip side, the optimal windowing function for the power spectrum will depend on the ALP coupling and the magnetic field strength. There is, in any case, a clear advantage of using the discrete power spectrum compared to a standard search for residual: While a high χ^2 value merely indicates that the data are more irregular than expected, a signal in the discrete power spectrum is a clear indication that the data have wiggles with the same energy dependence as expected for photon-ALP oscillations.

In this section, we have considered an optimistic value for the intergalactic magnetic field, $B_{\mathrm{rms}} = 5 \times 10^{-9}\,\mathrm{G}$, and an excluded coupling strength, $g_{a\gamma} = 10^{-11}\,\mathrm{GeV}^{-1}$. It is thus useful to check to what extent the detectability worsens when the magnetic field strength is decreased.[9] Therefore, we plot in figure 9 the histograms of the TS obtained for varying magnetic field strength, $B_{\mathrm{rms}} = \{5, 1, 0.5\}\,\mathrm{nG}$. The corresponding detection probabilities are $C_{95} = \{0.947, 0.547, 0.521\}$. Two effects lead to the quick reduction in C_{95} with decreasing magnetic field strength: First, the wiggles are strongest close to the strong mixing regime, and decreasing the magnetic field strength shifts the strong mixing regime to lower energies. From the condition in eq. (2.9), it is expected that our choice of default parameters leads to the strongest wiggles. This reduction in sensitivity may be partly compensated for by changing the lowest energy considered, for example by considering a different detector. Second, the mixing strength is proportional to the magnetic field strength, which can only be compensated for by increasing the observation time. At lower energies, however, the number of photons is usually significantly higher.

5 Summary and conclusion

Photon-ALP oscillations will imprint energy-dependent oscillatory features, which we name "ALP wiggles", on photon spectra from distant high-energy sources. We have therefore proposed to use the discrete power spectrum (3.3) to directly probe such wiggles in experimental data. Such a search will be independent of the modelling of magnetic fields and theoretical uncertainties in, e.g., the EBL. This work serves as a first proof of principle, and

[9] Since the oscillation depend on the magnetic field and the coupling strength via the combination $g_{a\gamma}B$, this is equivalent to reducing the coupling.

JCAP01(2024)044

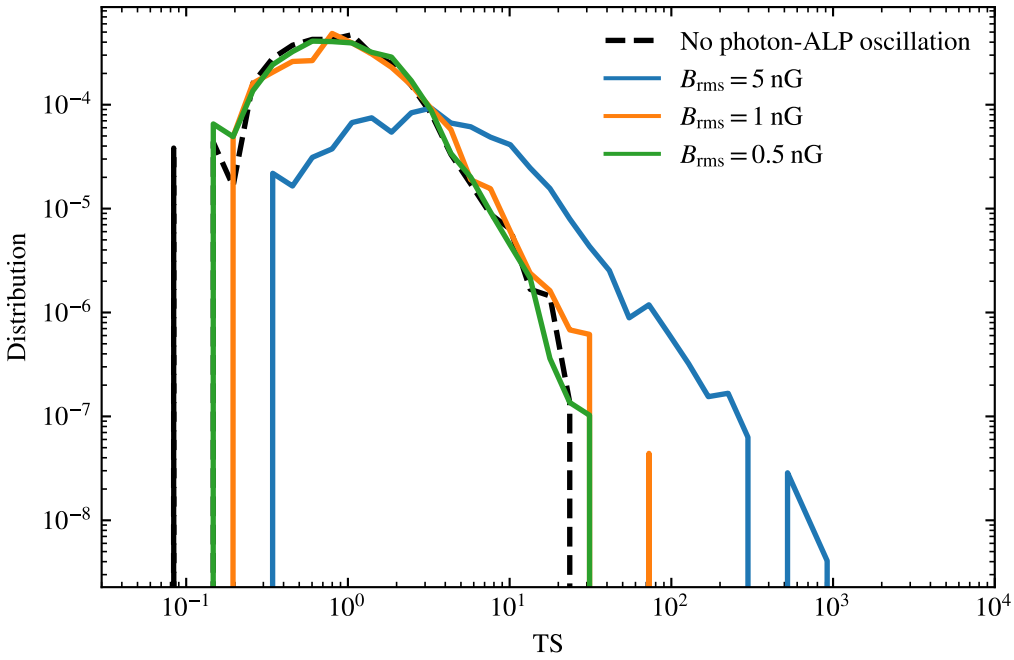

Figure 9. Histograms of the TS (3.4) obtained using the statistical method described in subsection 3.3 on the simulated data from PKS 2155-304 for an observation time $\Delta t = 200\,\mathrm{h}$. The results obtained with magnetic field strengths $B_{\rm rms} = 5\,\mathrm{nG}$ (blue), $B_{\rm rms} = 1\,\mathrm{nG}$ (orange) and $B_{\rm rms} = 0.5\,\mathrm{nG}$ (green) are shown. The no-ALP scenario is shown in dashed line.

there is room for improvement: We only considered the simple test statistic (3.4) which only measures the residual of the measured discrete power spectrum compared to the estimated background. Furthermore, in order to stay as concrete as possible, and since the onset of the ALP wiggles at TeV energies is determined by the weakest magnetic field that contribute to the oscillations, we considered only an intergalactic magnetic field. In a complete analysis, one should furthermore consider photon-ALP oscillations in, e.g., the Milky Way and the host galaxy, and in the source itself. As a second step, the discrete power spectrum can be used to extract information about the magnetic field, more specifically, it can be related to the two-point correlation function of the magnetic field [47, 72].

We have compared two different treatments of the magnetic field: a Gaussian turbulent field, and a simple and unphysical domain-like field. We found that the increased cosmic variance of the Gaussian turbulent field may significantly improve the detection prospects. Varying the shape of its power spectrum, we did not observe a strong dependence on the resulting axion wiggles, as long as the effective coherence length remained constant.

As a concrete example, we considered the detection of ALP wiggles in the energy spectrum from PKS 2155-304 using conservative estimates of the Cherenkov Telescope Array (CTA) sensitivity. Our analysis indicates that ALP wiggles can be detected by CTA for optimistic values of the magnetic field and photon-ALP coupling. Importantly, the method is an improvement compared to a standard search for "irregularities" in photon spectra, which is currently used to set leading limits. The statistical method can furthermore be optimised choosing an appropriate windowing function: Since the extragalactic magnetic field strength

JCAP01(2024)044

currently is only weakly constrained, one cannot know at which energy the first ALP wiggle occur. Moreover, the simple test statistic considered does not take into account the size, shape and location of the peak.

Acknowledgments

We would like to thank M. Unger for valuable discussions that helped to reduce the computational time required for generating the Gaussian turbulent fields. JT would like to thank M. Meyer for interesting discussions and hospitality at the University of Hamburg. This article is based upon work from the COST Action COSMIC WISPers CA21106, supported by COST (European Cooperation in Science and Technology).

References

[1] R.D. Peccei and H.R. Quinn, *CP Conservation in the Presence of Instantons*, *Phys. Rev. Lett.* **38** (1977) 1440 [INSPIRE].

[2] R.D. Peccei and H.R. Quinn, *Constraints Imposed by CP Conservation in the Presence of Instantons*, *Phys. Rev. D* **16** (1977) 1791 [INSPIRE].

[3] J. Preskill, M.B. Wise and F. Wilczek, *Cosmology of the Invisible Axion*, *Phys. Lett. B* **120** (1983) 127 [INSPIRE].

[4] L.F. Abbott and P. Sikivie, *A Cosmological Bound on the Invisible Axion*, *Phys. Lett. B* **120** (1983) 133 [INSPIRE].

[5] M. Dine and W. Fischler, *The Not So Harmless Axion*, *Phys. Lett. B* **120** (1983) 137 [INSPIRE].

[6] S. Weinberg, *A New Light Boson?*, *Phys. Rev. Lett.* **40** (1978) 223 [INSPIRE].

[7] F. Wilczek, *Problem of Strong P and T Invariance in the Presence of Instantons*, *Phys. Rev. Lett.* **40** (1978) 279 [INSPIRE].

[8] G. Grilli di Cortona, E. Hardy, J. Pardo Vega and G. Villadoro, *The QCD axion, precisely*, *JHEP* **01** (2016) 034 [arXiv:1511.02867] [INSPIRE].

[9] L. Di Luzio, M. Giannotti, E. Nardi and L. Visinelli, *The landscape of QCD axion models*, *Phys. Rept.* **870** (2020) 1 [arXiv:2003.01100] [INSPIRE].

[10] A. Arvanitaki et al., *String Axiverse*, *Phys. Rev. D* **81** (2010) 123530 [arXiv:0905.4720] [INSPIRE].

[11] M. Cicoli, M. Goodsell and A. Ringwald, *The type IIB string axiverse and its low-energy phenomenology*, *JHEP* **10** (2012) 146 [arXiv:1206.0819] [INSPIRE].

[12] S. Alexander, H. Gilmer, T. Manton and E. McDonough, *π-axion and π-axiverse of dark QCD*, *Phys. Rev. D* **108** (2023) 123014 [arXiv:2304.11176] [INSPIRE].

[13] P.W. Graham et al., *Experimental Searches for the Axion and Axion-Like Particles*, *Ann. Rev. Nucl. Part. Sci.* **65** (2015) 485 [arXiv:1602.00039] [INSPIRE].

[14] I.G. Irastorza and J. Redondo, *New experimental approaches in the search for axion-like particles*, *Prog. Part. Nucl. Phys.* **102** (2018) 89 [arXiv:1801.08127] [INSPIRE].

[15] CAST collaboration, *New CAST Limit on the Axion-Photon Interaction*, *Nature Phys.* **13** (2017) 584 [arXiv:1705.02290] [INSPIRE].

[16] A. Ayala et al., *Revisiting the bound on axion-photon coupling from Globular Clusters*, *Phys. Rev. Lett.* **113** (2014) 191302 [arXiv:1406.6053] [INSPIRE].

JCAP01(2024)044

[17] M.J. Dolan, F.J. Hiskens and R.R. Volkas, *Advancing globular cluster constraints on the axion-photon coupling*, *JCAP* **10** (2022) 096 [arXiv:2207.03102] [INSPIRE].

[18] R. Bähre et al., *Any light particle search II —Technical Design Report*, 2013 *JINST* **8** T09001 [arXiv:1302.5647] [INSPIRE].

[19] IAXO collaboration, *Physics potential of the International Axion Observatory (IAXO)*, *JCAP* **06** (2019) 047 [arXiv:1904.09155] [INSPIRE].

[20] ADMX collaboration, *Extended Search for the Invisible Axion with the Axion Dark Matter Experiment*, *Phys. Rev. Lett.* **124** (2020) 101303 [arXiv:1910.08638] [INSPIRE].

[21] J.L. Ouellet et al., *First Results from ABRACADABRA-10 cm: A Search for Sub-μeV Axion Dark Matter*, *Phys. Rev. Lett.* **122** (2019) 121802 [arXiv:1810.12257] [INSPIRE].

[22] J.W. Foster et al., *Extraterrestrial Axion Search with the Breakthrough Listen Galactic Center Survey*, *Phys. Rev. Lett.* **129** (2022) 251102 [arXiv:2202.08274] [INSPIRE].

[23] R.A. Battye et al., *Searching for time-dependent axion dark matter signals in pulsars*, *Phys. Rev. D* **108** (2023) 063001 [arXiv:2303.11792] [INSPIRE].

[24] H.E.S.S. collaboration, *Constraints on axionlike particles with H.E.S.S. from the irregularity of the PKS 2155-304 energy spectrum*, *Phys. Rev. D* **88** (2013) 102003 [arXiv:1311.3148] [INSPIRE].

[25] Fermi-LAT collaboration, *Search for Spectral Irregularities due to Photon-Axionlike-Particle Oscillations with the Fermi Large Area Telescope*, *Phys. Rev. Lett.* **116** (2016) 161101 [arXiv:1603.06978] [INSPIRE].

[26] C. Eckner and F. Calore, *First constraints on axionlike particles from Galactic sub-PeV gamma rays*, *Phys. Rev. D* **106** (2022) 083020 [arXiv:2204.12487] [INSPIRE].

[27] J.S. Reynés et al., *New constraints on light axion-like particles using Chandra transmission grating spectroscopy of the powerful cluster-hosted quasar H1821+643*, *Mon. Not. Roy. Astron. Soc.* **510** (2021) 1264 [arXiv:2109.03261] [INSPIRE].

[28] J.H. Matthews et al., *How Do Magnetic Field Models Affect Astrophysical Limits on Light Axion-like Particles? An X-Ray Case Study with NGC 1275*, *Astrophys. J.* **930** (2022) 90 [arXiv:2202.08875] [INSPIRE].

[29] C.S. Reynolds et al., *Astrophysical limits on very light axion-like particles from Chandra grating spectroscopy of NGC 1275*, *Astrophys. J.* **890** (2020) 59 [arXiv:1907.05475] [INSPIRE].

[30] CTA collaboration, *Sensitivity of the Cherenkov Telescope Array for probing cosmology and fundamental physics with gamma-ray propagation*, *JCAP* **02** (2021) 048 [arXiv:2010.01349] [INSPIRE].

[31] A. Payez et al., *Revisiting the SN1987A gamma-ray limit on ultralight axion-like particles*, *JCAP* **02** (2015) 006 [arXiv:1410.3747] [INSPIRE].

[32] M. Xiao et al., *Constraints on Axionlike Particles from a Hard X-Ray Observation of Betelgeuse*, *Phys. Rev. Lett.* **126** (2021) 031101 [arXiv:2009.09059] [INSPIRE].

[33] C. Dessert, J.W. Foster and B.R. Safdi, *X-ray Searches for Axions from Super Star Clusters*, *Phys. Rev. Lett.* **125** (2020) 261102 [arXiv:2008.03305] [INSPIRE].

[34] D. Noordhuis et al., *Novel Constraints on Axions Produced in Pulsar Polar-Cap Cascades*, *Phys. Rev. Lett.* **131** (2023) 111004 [arXiv:2209.09917] [INSPIRE].

[35] G. Galanti, *Photon-ALP oscillations inducing modifications to photon polarization*, *Phys. Rev. D* **107** (2023) 043006 [arXiv:2202.11675] [INSPIRE].

JCAP01(2024)044

[36] D. Lai and J. Heyl, *Probing Axions with Radiation from Magnetic Stars*, *Phys. Rev. D* **74** (2006) 123003 [astro-ph/0609775] [INSPIRE].

[37] R. Gill and J.S. Heyl, *Constraining the photon-axion coupling constant with magnetic white dwarfs*, *Phys. Rev. D* **84** (2011) 085001 [arXiv:1105.2083] [INSPIRE].

[38] C. Dessert, D. Dunsky and B.R. Safdi, *Upper limit on the axion-photon coupling from magnetic white dwarf polarization*, *Phys. Rev. D* **105** (2022) 103034 [arXiv:2203.04319] [INSPIRE].

[39] A. De Angelis, M. Roncadelli and O. Mansutti, *Evidence for a new light spin-zero boson from cosmological gamma-ray propagation?*, *Phys. Rev. D* **76** (2007) 121301 [arXiv:0707.4312] [INSPIRE].

[40] S. Jacobsen, T. Linden and K. Freese, *Constraining axion-like particles with HAWC observations of TeV blazars*, *JCAP* **10** (2023) 009 [arXiv:2203.04332] [INSPIRE].

[41] J. Davies, M. Meyer and G. Cotter, *Constraints on axionlike particles from a combined analysis of three flaring Fermi flat-spectrum radio quasars*, *Phys. Rev. D* **107** (2023) 083027 [arXiv:2211.03414] [INSPIRE].

[42] A. Kartavtsev, G. Raffelt and H. Vogel, *Extragalactic photon-ALP conversion at CTA energies*, *JCAP* **01** (2017) 024 [arXiv:1611.04526] [INSPIRE].

[43] D. Montanino, F. Vazza, A. Mirizzi and M. Viel, *Enhancing the Spectral Hardening of Cosmic TeV Photons by Mixing with Axionlike Particles in the Magnetized Cosmic Web*, *Phys. Rev. Lett.* **119** (2017) 101101 [arXiv:1703.07314] [INSPIRE].

[44] M. Libanov and S. Troitsky, *On the impact of magnetic-field models in galaxy clusters on constraints on axion-like particles from the lack of irregularities in high-energy spectra of astrophysical sources*, *Phys. Lett. B* **802** (2020) 135252 [arXiv:1908.03084] [INSPIRE].

[45] P. Carenza et al., *Turbulent axion-photon conversions in the Milky Way*, *Phys. Rev. D* **104** (2021) 023003 [arXiv:2104.13935] [INSPIRE].

[46] M. Meyer, D. Montanino and J. Conrad, *On detecting oscillations of gamma rays into axion-like particles in turbulent and coherent magnetic fields*, *JCAP* **09** (2014) 003 [arXiv:1406.5972] [INSPIRE].

[47] M. Kachelriess and J. Tjemsland, *On the origin and the detection of characteristic axion wiggles in photon spectra*, *JCAP* **01** (2022) 025 [arXiv:2111.08303] [INSPIRE].

[48] G. Raffelt and L. Stodolsky, *Mixing of the Photon with Low Mass Particles*, *Phys. Rev. D* **37** (1988) 1237 [INSPIRE].

[49] A. Dobrynina, A. Kartavtsev and G. Raffelt, *Photon-photon dispersion of TeV gamma rays and its role for photon-ALP conversion*, *Phys. Rev. D* **91** (2015) 083003 [*Erratum ibid.* **95** (2017) 109905] [arXiv:1412.4777] [INSPIRE].

[50] M. Kachelriess, S. Ostapchenko and R. Tomàs, *ELMAG: A Monte Carlo simulation of electromagnetic cascades on the extragalactic background light and in magnetic fields*, *Comput. Phys. Commun.* **183** (2012) 1036 [arXiv:1106.5508] [INSPIRE].

[51] M. Blytt, M. Kachelriess and S. Ostapchenko, *ELMAG 3.01: A three-dimensional Monte Carlo simulation of electromagnetic cascades on the extragalactic background light and in magnetic fields*, arXiv:1909.09210 [DOI:10.1016/j.cpc.2020.107163] [INSPIRE].

[52] M. Meyer, J. Davies and J. Kuhlmann, *gammaALPs: An open-source python package for computing photon-axion-like-particle oscillations in astrophysical environments*, *PoS* **ICRC2021** (2021) 557 [arXiv:2108.02061] [INSPIRE].

[53] R. Alves Batista and A. Saveliev, *The Gamma-ray Window to Intergalactic Magnetism*, *Universe* **7** (2021) 223 [arXiv:2105.12020] [INSPIRE].

JCAP01(2024)044

[54] R. Durrer and A. Neronov, *Cosmological Magnetic Fields: Their Generation, Evolution and Observation*, *Astron. Astrophys. Rev.* **21** (2013) 62 [arXiv:1303.7121] [INSPIRE].

[55] J. Giacalone and J.R. Jokipii, *Charged-particle motion in multidimensional magnetic-field turbulence*, *Astrophys. J. Lett.* **430** (1994) L137.

[56] J. Giacalone and J.R. Jokipii, *The Transport of Cosmic Rays across a Turbulent Magnetic Field*, *Astrophys. J.* **520** (1999) 204.

[57] G. Galanti and M. Roncadelli, *Behavior of axionlike particles in smoothed out domainlike magnetic fields*, *Phys. Rev. D* **98** (2018) 043018 [arXiv:1804.09443] [INSPIRE].

[58] G. Galanti and M. Roncadelli, *Extragalactic photon-axion-like particle oscillations up to 1000 TeV*, *JHEAp* **20** (2018) 1 [arXiv:1805.12055] [INSPIRE].

[59] D. Wouters and P. Brun, *Irregularity in gamma ray source spectra as a signature of axionlike particles*, *Phys. Rev. D* **86** (2012) 043005 [arXiv:1205.6428] [INSPIRE].

[60] A. De Angelis, G. Galanti and M. Roncadelli, *Relevance of axion-like particles for very-high-energy astrophysics*, *Phys. Rev. D* **84** (2011) 105030 [*Erratum ibid.* **87** (2013) 109903] [arXiv:1106.1132] [INSPIRE].

[61] G. Galanti, F. Tavecchio, M. Roncadelli and C. Evoli, *Blazar VHE spectral alterations induced by photon-ALP oscillations*, *Mon. Not. Roy. Astron. Soc.* **487** (2019) 123 [arXiv:1811.03548] [INSPIRE].

[62] H.E.S.S. and FERMI-LAT collaborations, *Constraints on the Intergalactic Magnetic Field Using Fermi-LAT and H.E.S.S. Blazar Observations*, *Astrophys. J. Lett.* **950** (2023) L16 [arXiv:2306.05132] [INSPIRE].

[63] A. Neronov and I. Vovk, *Evidence for strong extragalactic magnetic fields from Fermi observations of TeV blazars*, *Science* **328** (2010) 73 [arXiv:1006.3504] [INSPIRE].

[64] K. Dolag, M. Kachelriess, S. Ostapchenko and R. Tomàs, *Lower limit on the strength and filling factor of extragalactic magnetic fields*, *Astrophys. J. Lett.* **727** (2011) L4 [arXiv:1009.1782] [INSPIRE].

[65] M.S. Pshirkov, P.G. Tinyakov and F.R. Urban, *New limits on extragalactic magnetic fields from rotation measures*, *Phys. Rev. Lett.* **116** (2016) 191302 [arXiv:1504.06546] [INSPIRE].

[66] A.E. Broderick et al., *Missing Gamma-ray Halos and the Need for New Physics in the Gamma-ray Sky*, *Astrophys. J.* **868** (2018) 87 [arXiv:1808.02959] [INSPIRE].

[67] J.P. Conlon and M. Rummel, *Improving Statistical Sensitivity of X-ray Searches for Axion-Like Particles*, *Mon. Not. Roy. Astron. Soc.* **484** (2019) 3573 [arXiv:1808.05916] [INSPIRE].

[68] P. Carenza et al., *Magnetohydrodynamics predicts heavy-tailed distributions of axion-photon conversion*, *Phys. Rev. D* **108** (2023) 103029 [arXiv:2208.04333] [INSPIRE].

[69] F. Aharonian et al., *An Exceptional Very High Energy Gamma-Ray Flare of PKS 2155-304*, *Astrophys. J. Lett.* **664** (2007) L71 [arXiv:0706.0797] [INSPIRE].

[70] Q. Yu and D. Horns, *Searching for photon-ALPs mixing effects in AGN gamma-ray energy spectra*, *JCAP* **05** (2023) 029 [arXiv:2208.00079] [INSPIRE].

[71] CTA CONSORTIUM collaboration, *Performance of the Cherenkov Telescope Array*, *PoS* **ICRC2019** (2020) 733 [arXiv:1907.08171] [INSPIRE].

[72] M.C.D. Marsh, J.H. Matthews, C. Reynolds and P. Carenza, *Fourier formalism for relativistic axion-photon conversion with astrophysical applications*, *Phys. Rev. D* **105** (2022) 016013 [arXiv:2107.08040] [INSPIRE].

JCAP01(2024)044